Journal of Photochemistry and Photobiology A: Chemistry 203 (2009) 112–118

Contents lists available at ScienceDirect

Journal of Photochemistry and Photobiology A: Chemistry

journal homepage: www.elsevier.com/locate/jphotochem

Photoactive component-loaded Nafion film as a platform of hydrogen generation: Alternative utilization of a classical sensitizing system

Hyunwoong Park[a,b], Yiseul Park[a], Eunyoung Bae[a], Wonyong Choi[a,*]

[a] School of Environmental Science and Engineering, Pohang University of Science and Technology (POSTECH), Hyoja-dong, Pohang 790-784, Republic of Korea
[b] School of Physics and Energy Science, Kyungpook National University, Daegu 702-701, Republic of Korea

ARTICLE INFO

Article history:
Received 1 September 2008
Received in revised form 5 December 2008
Accepted 29 December 2008
Available online 4 January 2009

Keywords:
Nafion film
Ruthenium bipyridyl sensitizer
Photocatalysis
Visible light
Hydrogen production

ABSTRACT

The photochemical hydrogen production was achieved by integrating photoactive components in a polymer membrane film under visible-light irradiation. The classical homogeneous photochemical system employing ruthenium bipyridyl complex ($Ru(bpy)_3^{2+}$) as a sensitizer, methyl viologen (MV^{2+}) as an electron shuttle, Pt as a hydrogen-evolving catalyst was heterogenized by immobilizing the active components within Nafion film. The integrated Nafion film provides a unique environment in which the immobilization of the components, light absorption, charge separation/transfer, and hydrogen production concur. The hydrogen evolution from the loaded Nafion film under visible light ($\lambda > 420$ nm) was successfully demonstrated. The loaded Pt particles were mainly located at the external surface of the film while the sensitizer was bound at the cation-exchange sites in the nanoporous channel. The electron-relaying action of MV^{2+} was effective only above 1 mM because most MV^{2+} ions below this concentration were bound at the ion-exchange site with restricted mobility. The effects of various components on the hydrogen production in this heterogenized system were investigated and discussed. The present Nafion film system may serve as a prototype of solar hydrogen generating films and can be further modified and optimized for practical applications.

1. Introduction

Photochemical systems harvesting visible light have employed a variety of semiconductors, metal–organic complexes, and organic dyes as a light absorbing unit [1–5]. Among them, Ru-complex and its derivatives have been widely investigated as one of the most efficient photosensitizer for solar energy conversion [1,2,6–10]. In the Ru-complex sensitized systems for hydrogen production, the effects of various parameters such as the kind of ligands, solvents, electron donors, electron mediators, and noble metal colloids were investigated [1,2]. The quantum yields for hydrogen production widely vary depending on the system conditions in the range of 0.05–53% [1,2]. The homogeneous sensitizing system, however, suffers from the dimerization of sensitizers and coagulation with catalysts (e.g., Pt colloid) [3]. In addition, the need of recovery of the sensitizers and catalysts makes the system less practical [11]. To overcome this limitation, it is required to immobilize or anchor the active components on inorganic/organic supports (e.g., zeolite, titania [8,9], cellulose [12], micelle [13], chelating resin [14], polymer [15–22]).

Nafion (Nf), a cation-exchanging polymer, has well-organized hydrophilic pore (~4 nm) structure surrounded by sulfonic anion groups ($-SO_3^-$) [23] that are linked to hydrophobic fluorocarbon chains (i.e., inverted micelle clusters composed of the sulfonic groups). Due to the high stability, it is often used as a supporting material for anchoring cationic components in photochemical conversion systems [24–26]. The presence of Nf adlayers on TiO_2 particles significantly enhanced the photocatalytic degradation of cationic substrates by holding them within the Nf layer close to the TiO_2 surface [24]. $Ru(bpy)_3^{2+}$, which does not bind to the TiO_2 surface at all, can be anchored on the Nf-coated Pt/TiO_2 surface through the ion exchange, which enabled the efficient production of H_2 under visible light [25].

The immobilization of Ru-bipyridyl complex ($Ru^{II}L_x$), methyl viologen (MV^{2+}), and Pt nanoparticle into a cation-exchange polymer film has been often suggested as a method for the visible-light-induced hydrogen production [3,14–21,26]. However, most studies have focused on the adsorption/desorption of the cationic components within the polymer film, the electrochemical behaviors of $Ru^{II}L_x$ immobilized on a polymer-coated electrode, and the photo-induced charge transfer between $Ru^{II}L_x$ and MV^{2+} in a polymer membrane. Only a few reports investigated the photochemical conversion reaction in the $Ru^{II}L_x$/polymer hybrid system. For example, Shiroishi et al. reported visible-light driven H_2 production using $Ru(dcbpy)_3$/Nf film with a very low efficiency (the hydrogen production rate of $\sim 7 \times 10^{-9}$ mol cm^{-2} h^{-1}) [18]. Hirose et al. compared the photoactivity of $Co(bpy)_3^{2+}$ and $Ru(bpy)_3^{2+}$

* Corresponding author. Tel.: +82 54 279 2283; fax: +82 54 279 8299.
E-mail address: wchoi@postech.edu (W. Choi).

1010-6030/$ – see front matter © 2009 Elsevier B.V. All rights reserved.
doi:10.1016/j.jphotochem.2008.12.025

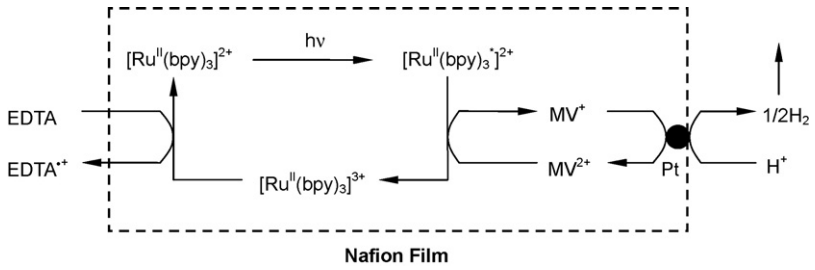

Scheme 1. Schematic diagram of the heterogenized sensitizing system in which photoactive components are immobilized in Nf film for H_2 production under visible-light irradiation.

attached to cation-exchange polymer (Amberlite) for CO_2 reduction and H_2 production under UV irradiation [19]. Similarly, Kurimura et al. observed the production of H_2O_2 from O_2 on the visible-light-irradiated $Ru(bpy)_3^{2+}$/(chelate resin-coated bead) [14]. All the previous studies on the immobilized system containing the Ru-complex, however, provided very limited information about how each active component is related with the overall sensitization process and what parameter is critical.

In this study, we systematically investigated a two-dimensionally heterogenized system in which Pt nanoparticles and $Ru(bpy)_3^{2+}$ sensitizers were immobilized on Nf film as a platform of photochemical conversion (Scheme 1). Pt nanoparticles were deposited on the external surface of the Nf film and were spatially separated from $Ru(bpy)_3^{2+}$ and MV^{2+} which were preferentially anchored within the film bulk. The hydrogen production from the Nf film that integrated the classical sensitizing system was successfully demonstrated under visible-light irradiation. The effects of the active components on the photoconversion efficiency were discussed and compared with those in the well-known homogeneous sensitizing system.

2. Experimental

2.1. Chemicals

Tris(2,2′-bipyridyl)dichloro ruthenium(II) ($Ru(bpy)_3^{2+}$), methyl viologen dichloride (MV^{2+}), disodium ethylenediaminetetraacetate (EDTA), and tetraamine platinum(II) dichloride ($Pt(NH_3)_4Cl_2$) were purchased from Aldrich (all of reagent grade) and used without further treatment. Nf membrane (Nafion™ NE-1035: perfluorosulfonic acid-PTFE copolymer, ~90 μm thick, standard ion-exchange capacity 1.0 mequiv./g) was purchased from Alfa Aesar.

2.2. Sample preparation

A sheet of Nf membrane (15 cm × 15 cm) was cut into the size of 1.2 cm × 1.5 cm, which was boiled in a mixture of concentrated HNO_3 and water (1:1, v/v) until it became transparent. Then, it was boiled repeatedly in triply distilled water until pH of the water became neutral. The mass of the dried bare Nf film, {Nf}, was ca. 11 mg/cm^2. The {Nf} was immersed in the aqueous solution of $Pt(NH_3)_4Cl_2$ overnight to absorb the Pt-complex through ion exchange. The Pt loading was adjusted by changing $[Pt(NH_3)_4Cl_2]$ and was checked by analyzing the Pt concentration before and after the absorption using an inductively coupled plasma atomic emission spectrophotometer (ICP-AES). It was found that more than 97% of initial $Pt(NH_3)_4Cl_2$ was absorbed into {Nf}. This {Pt^{II}/Nf} was washed with distilled water and immersed in 50 mM $NaBH_4$ solution to reduce Pt^{II} to Pt^0 with ultrasonification. The ultrasonic treatment along with the chemical reduction made Pt^0 more uniformly distributed in {Nf} than the chemical reduction method alone. After the Pt reduction step, the transparent Nf film turned blackish. Then, $Ru(bpy)_3^{2+}$ was absorbed into the Pt^0-loaded Nf film, {Pt/Nf}, by immersing it in $Ru(bpy)_3^{2+}$ solution overnight in the dark. The $Ru(bpy)_3^{2+}$-absorbed film, {Ru^{II}/Pt/Nf}, was washed and stored in distilled water before use. During the storage in water, neither $Ru(bpy)_3^{2+}$ nor Pt-complex ion was leached out of the Nf film. The {Ru^{II}/Nf} was prepared in the same way without the Pt loading step.

2.3. Surface characterization

{Pt/Nf} films loaded with varying amount of Pt were prepared and analyzed with X-ray photoelectron spectroscopy (XPS, Kratos XSAM 800 pci) using Mg Kα lines (1253.6 eV) as an excitation source. The spectra were taken for each sample after Ar^+ (3 keV) sputter cleaning. Surface charging was minimized by spraying low energy electrons over the sample surface using a neutralizer gun. Binding energy (BE) spectra were recorded in the regions of Pt 4f. The BEs of all peaks were referenced against the F 1s line (688.7 eV) originating from the Nf surface fluorine. The surfaces of {Nf} and {Pt/Nf}, and their cross-section were analyzed with a field emission scanning electron microscope (FE-SEM, JEOL JSM 6330F).

2.4. Photochemical hydrogen production

The {Ru^{II}/Pt/Nf} film was placed and fixed on the bottom of a cylindrical pyrex reactor (10 mL). Desired amounts of MV^{2+} and EDTA solutions were added to the reactor up to 9 mL, and the reactor was sealed with septum and purged with N_2 gas for 30 min. An overnight equilibration was done for MV^{2+} absorption into the Nf matrix prior to irradiation. The initial solution pH was typically 5.8. A 450-W Xe arc lamp was used as a light source. Light passed through a 10-cm IR water filter and a cutoff filter (λ > 420 nm), and then the filtered visible light was focused onto the bottom face of the cylindrical reactor on which {Ru^{II}/Pt/Nf} was laid down. Light intensity was measured by chemical actinometry using (*E*)-α-(2,5-dimethyl-3-furylethylidene) (isopropylidene) succinic anhydride (Aberchrome 540) [27]. A typical incident light intensity was measured to be ca. 2×10^{-3} einstein L^{-1} min^{-1} in the wavelength range of 420–550 nm. The amount of H_2 produced in headspace was analyzed using a HP6890A GC equipped with a TCD detector and a molecular sieve 5A column.

3. Results and discussion

3.1. Nafion film immobilized with the active components

Fig. 1a shows the UV–vis absorption spectra of the {Pt/Nf} as a function of the Pt load. Bare {Nf} without Pt was almost transparent indicating the absence of impurities within {Nf}. The chemical reduction of Pt^{II} changed the color of {Nf} blackish as a result of the formation of Pt^0 particles and the color became darker with increasing the Pt loading. The absorption/scattering background is extended throughout the entire wavelength range. Fig. 1b compares UV–vis absorption spectra of {Nf}, {Pt/Nf}, {Ru^{II}/Pt/Nf} films along

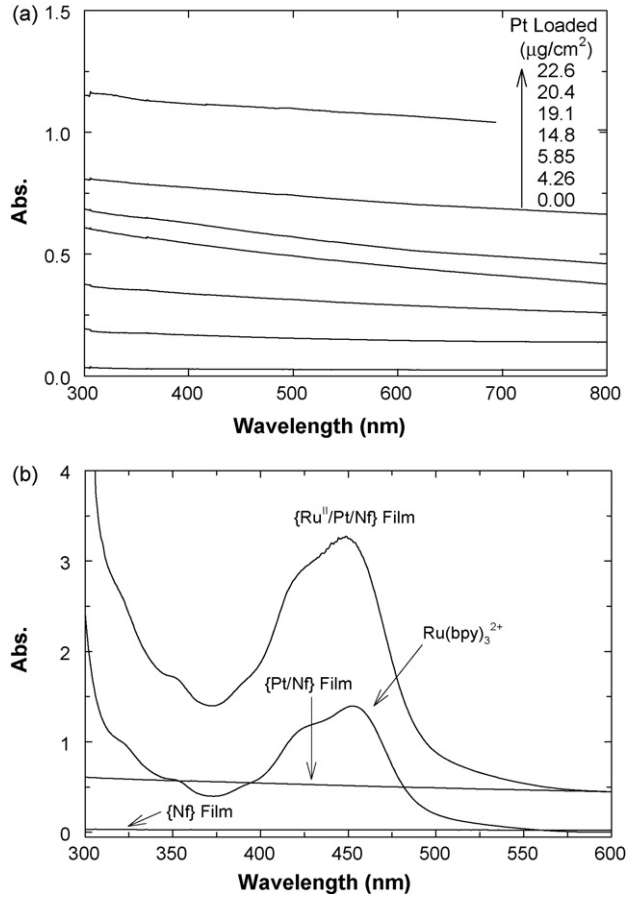

Fig. 1. (a) UV–vis absorption spectra of Pt^0-loaded Nf film as a function of the Pt loading that is expressed in terms of the pre-absorbed concentration of Pt^{II}. (b) UV–vis absorption spectra of {Nf}, {Pt/Nf}, {Ru^{II}/Pt/Nf} films, and aqueous solution of $Ru(bpy)_3^{2+}$ (100 μM). $[Pt^{II}]_{Nf}$ = 14.8 μg/cm² (0.076 μmol/cm²); $[Ru(bpy)_3^{2+}]_{Nf}$ = 0.43 μmol/cm².

with that of $Ru(bpy)_3^{2+}$ solution. The {Ru^{II}/Pt/Nf} exhibited a metal-to-ligand charge transfer (MLCT) absorption band (λ_{max} = 449 nm) due to the presence of $Ru(bpy)_3^{2+}$ absorbed in the Nf matrix. $Ru(bpy)_3^{2+}$ is attached to the sulfonate group by the electrostatic force while the bipyridyl ligands may have a hydrophobic interaction with the fluorocarbon backbones [20].

FE-SEM images of {Nf} and {Pt/Nf} show that the surface of {Nf} and {Pt^{II}/Nf} was plain whereas that of the chemically reduced {Pt^0/Nf} appeared dramatically different (Fig. 2). Pt particles of 50–500 nm in size were formed on the {Nf} surface (not inside the {Nf}) after the chemical reduction. Pt^{II} precursor ions are initially dispersed and bound to the sulfonate groups within the Nf matrix. During the chemical reduction, Pt^{II} ions are transformed to Pt^0 nanoparticles. However, as the Pt particles grow larger than the size of pores (~4 nm) in the Nf film, they are gradually pushed up from the inner matrix onto the external surface through the ionic channels with aggregating themselves (Scheme 2). The exposed Pt particles are observed in the SEM image of {Pt/Nf} (Fig. 2d and f). The energy dispersive X-ray (EDX) analysis of {Pt/Nf} also confirms the presence of Pt as well as F and S that are the elemental components of Nf (Fig. 3a).

To investigate the chemical states of the Pt, the surface of {Pt/Nf} samples prepared with different chemical reduction time were analyzed with XPS (Fig. 3b). The chemical reduction time less than 3 min produced little sign of the surface Pt whereas the longer reduction time markedly increased the Pt band [Pt^0 $4f_{7/2}$ (71.5 eV) and $4f_{5/2}$ (74.8 eV)]. Although all {Pt/Nf} films have the same load

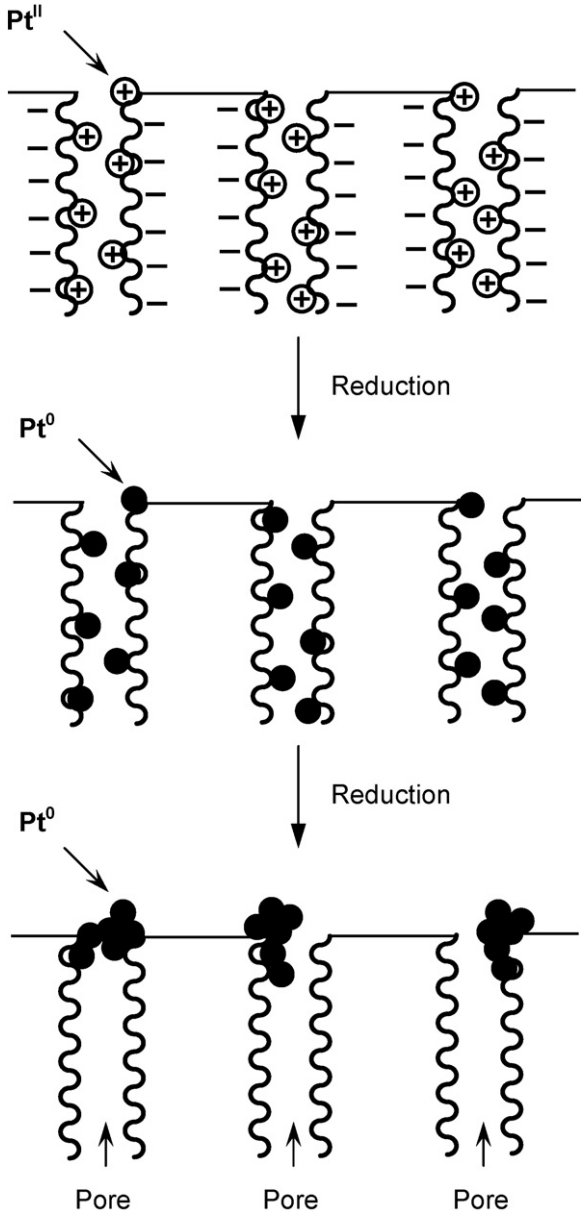

Scheme 2. Schematic illustration that describes the process of Pt^0 particle formation within the Nf matrix.

of Pt^{II} precursor ions, the surface Pt concentration is very different depending on the chemical reduction time. This indicates that the Pt ions present inside the Nf film gradually move onto the external surface as the reduced Pt^0 particles grow larger.

3.2. Heterogenized vs. homogeneous systems

The H_2 production in the well-known homogeneous sensitizing system proceeds as follows (Reactions (1)–(6)):

$$Ru(bpy)_3^{2+} + h\upsilon \rightarrow Ru(bpy)_3^{2+*}, \quad I_a \tag{1}$$

$$Ru(bpy)_3^{2+*} \rightarrow Ru(bpy)_3^{2+}, \quad k_f = 1.6 \times 10^6\ s^{-1} \tag{2}$$

$$Ru(bpy)_3^{2+*} + MV^{2+} \rightarrow Ru(bpy)_3^{3+} + MV^{\bullet+}, \quad k_{et} = 5.0 \times 10^8\ M^{-1}\ s^{-1} \tag{3}$$

$$Ru(bpy)_3^{3+} + MV^{\bullet+} \rightarrow Ru(bpy)_3^{2+} + MV^{2+}, \quad k_b = 2.9 \times 10^9\ M^{-1}\ s^{-1} \tag{4}$$

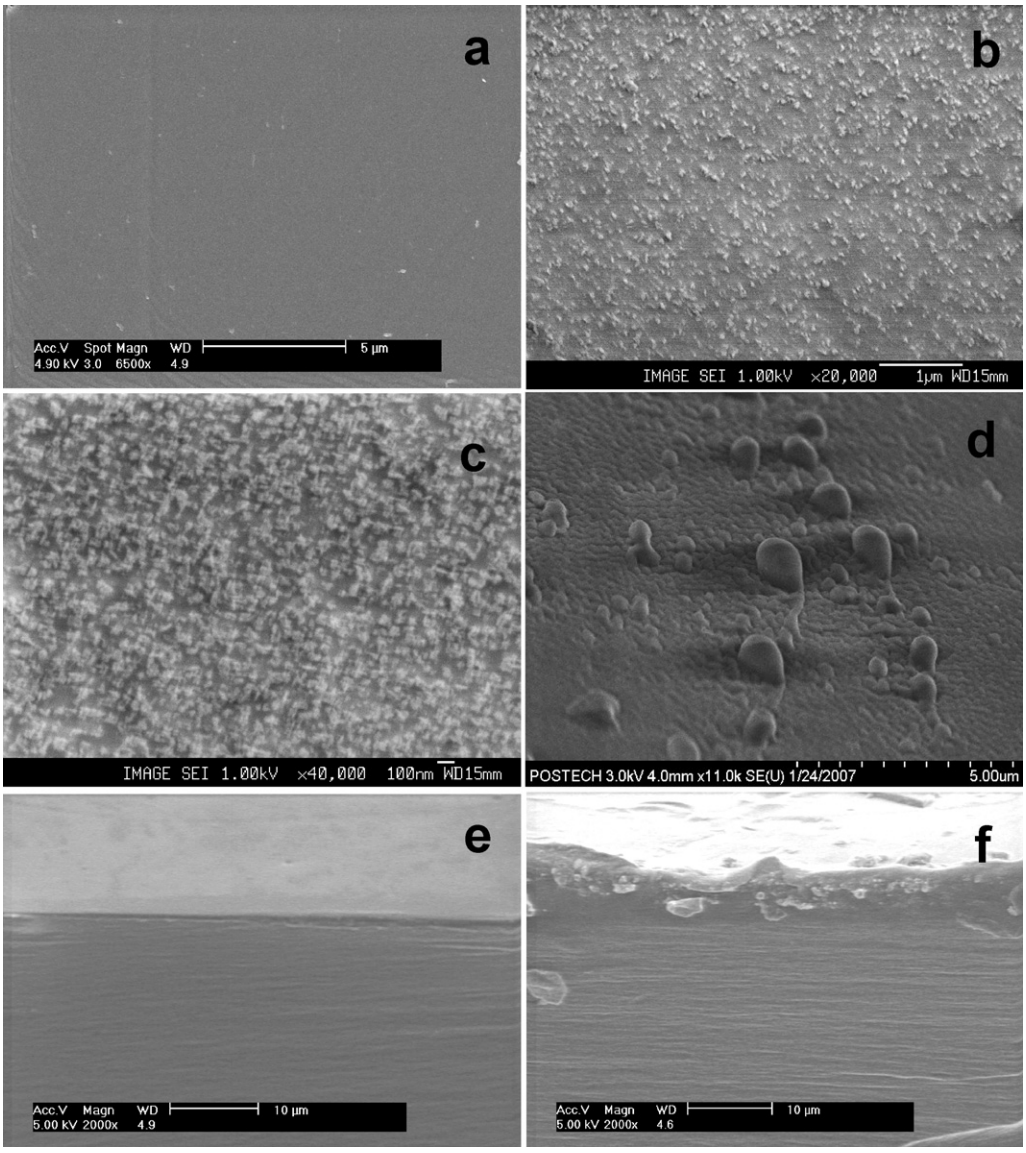

Fig. 2. SEM images of (a) Pt^{II}-loaded Nf film (top view); (b and c) Pt^{0}-loaded Nafion film after 10 min of chemical reduction (top view); (d) Pt^{0}-loaded Nafion film after 15 min of chemical reduction (top view); (e) Pt^{II}-loaded Nafion film (cross-sectional view); (f) Pt^{0}-loaded Nafion film after 15 min of chemical reduction (cross-sectional view).

$$Ru(bpy)_3{}^{3+} + EDTA \rightarrow Ru(bpy)_3{}^{2+} + EDTA^{\bullet+},$$
$$k_{rg} = 1.1 \times 10^8\ M^{-1}\ s^{-1} \quad (5)$$

$$2MV^{\bullet+} + 2H_2O\,(\text{at Pt}) \rightarrow 2MV^{2+} + H_2 + 2OH^-, \quad k_{\text{hetero},H_2} \quad (6)$$

Each component has a significant effect on the hydrogen production in the homogeneous sensitizing system (see Figs. S1–S4 in electronic supplementary information). The Pt sol has an optimal concentration around 1 mg cm^{-3} (Fig. S1) while the increase of [$Ru(bpy)_3{}^{2+}$] or [EDTA] reached the plateau region of the hydrogen production (Figs. S2 and S4). As for MV^{2+}, the hydrogen production rate was optimized at 4 mM (Fig. S3).

The general photochemical mechanism is likely to be similar in the heterogenized system as well. The typical time profiles of hydrogen production under visible light are shown in Fig. 4a. The hydrogen production on {Ru^{II}/Nf} without Pt is insignificant. The hydrogen production rate initially increased with increasing Pt loading and then reached an optimal value above which further increase in Pt loading decreased the efficiency (Fig. 4b). The presence of the optimal Pt loading can be explained in terms of two factors: light shielding and the particle agglomeration. An excessive loading of Pt particles in both homogeneous (see Fig. S1) and heterogenized systems not only scatters or shields incoming light (see Fig. 1a) but also reduces the surface area by inducing Pt–Pt agglomeration (see Fig. 2d and f).

The concentrations of the sensitizer, the electron relay, and the electron donor also significantly affect the hydrogen production rate (Fig. 5a–c). The sensitizer loading up to ~0.7 μmol cm^{-2} in {Ru^{II}/Pt/Nf} gradually increases the hydrogen production rate. The dependence of the hydrogen production rate on [MV^{2+}] in the heterogenized system is very different from that of the homogeneous system. In the homogeneous solution, the rate of hydrogen production initially increases with [MV^{2+}] but decreases above [MV^{2+}] = 4 mM (Fig. S3). The rate of H_2 production should be proportional to the rate of MV^+ formation [29] The higher [MV^{2+}], the more MV^+s are generated (Reaction (3)). However, the generation of MV^+ molecules that are more than enough can hinder the overall sensitization by shielding visible light since both $Ru(bpy)_3{}^{2+}$ and MV^+ absorb visible light.

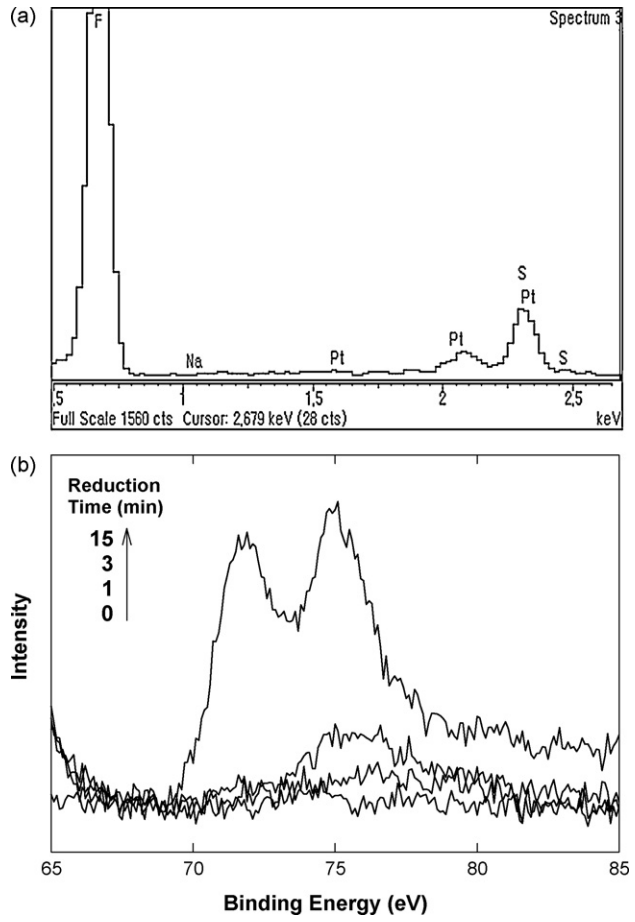

Fig. 3. (a) EDX analysis of Pt^0-loaded Nf film. $[Pt^0] = 14.8\ \mu g/cm^2$. (b) XPS spectra of Pt on {Pt/Nf} with varying the chemical reduction time. For all samples, the initially absorbed Pt^{II} precursor ions were the same at 14.8 μg/cm².

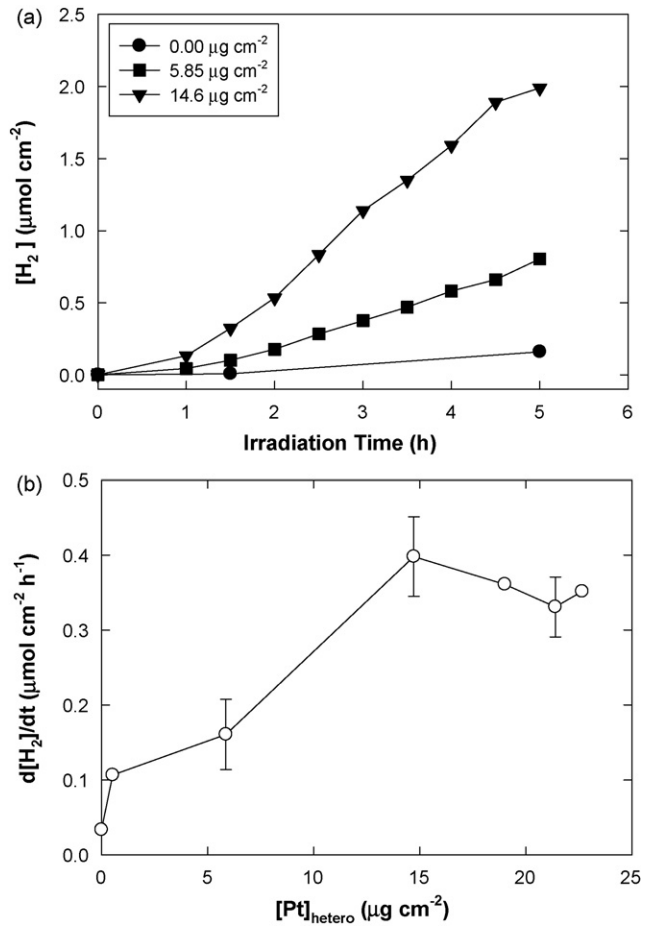

Fig. 4. (a) Time profiles of visible-light-induced H_2 production in the heterogenized $\{Ru^{II}/Pt/Nf\}$ film with different Pt loading. (b) The rate of H_2 production (averaged over 3–5 h) as a function of Pt loading in the heterogeneous systems. The experimental conditions were: $[Ru(bpy)_3^{2+}]_{Nf} = 0.43\ \mu mol/cm^2$; $[MV^{2+}] = 4$ mM; [EDTA] = 4 mM; visible-light ($\lambda > 420$ nm) irradiated.

On the other hand, in the heterogenized system, the hydrogen production started only with $[MV^{2+}] > 1$ mM and the retardation effect was not observed up to $[MV^{2+}] = 8$ mM (Fig. 5b). With $[MV^{2+}] \geq 6$ mM in the solution containing $\{Ru^{II}/Pt/Nf\}$, a small fraction of absorbed $Ru(bpy)_3^{2+}$ was leached out of Nf film because MV^{2+} displaced some $Ru(bpy)_3^{2+}$ in the cation-exchange sites. Rabani et al. also observed that the bound $Ru(bpy)_3^{2+}$ could be exchanged with MV^{2+} in an aqueous Nafion solution [15]. According to the manufacturer, the ion-exchange capacity of Nf film is ca. 1.0 mequiv./g, which corresponds to 11 μequiv./cm². In the present experimental condition, the ion-exchange sites occupied by $Ru(bpy)_3^{2+}$ in {Nf} are as low as 1 μequiv./cm². In the presence of 1 mM MV^{2+} (solution volume = 9 mL, total 18 μequiv.), the exchange sites of the Nf film (1.8 cm²), which are around 20 μequiv., are mostly occupied by MV^{2+}. Therefore, unbound MV^{2+} molecules that may diffuse freely through the pores of Nf membrane are available only when the total concentration of MV^{2+} is much higher than 1 mM. When most MV^{2+} molecules, the electron shuttles, are bound at the ion-exchange sites, their mobility within the Nf membrane is highly restricted and they cannot play the role of the electron shuttle efficiently. This is consistent with the fact that the hydrogen production in $\{Ru^{II}/Pt/Nf\}$ system with 1 mM MV^{2+} is completely absent whereas the homogeneous counterpart was quite effective in H_2 production with $[MV^{2+}] = 1$ mM. Therefore, the efficient hydrogen production in $\{Ru^{II}/Pt/Nf\}$ system is mediated by the unbound electron shuttles (MV^{2+}) that are available at $[MV^{2+}] > 1$ mM. In addition, it should be noted that the Nafion support provides a favorable environment for the electron transfer. As a result of the photo-induced electron transfer (Reaction (3)) in Nf film, $Ru(bpy)_3^{3+}$ and MV^+ are generated. The former is more bound to the sulfonate group (electrostatically) than $Ru(bpy)_3^{2+}$ while the latter is less bound and more mobile than MV^{2+}. The enhanced mobility of MV^+ in Nf film should increase the production of hydrogen.

The dependence of the H_2 production rate on [EDTA], the electron donor, is also different between the two systems. In the homogeneous solution, the hydrogen production rate rapidly increased when [EDTA] increased from 0 to 2 mM (Fig. S3) whereas that in the heterogenized system was much less efficient in the same concentration range of EDTA (Fig. 5c). However, in both systems the H_2 production rate was saturated at around [EDTA] = 4 mM. The low efficiency of EDTA as an electron donor below 2 mM in $\{Ru^{II}/Pt/Nf\}$ system may be due to the hindered accessibility of EDTA anions, which are present predominantly as anionic forms (H_2Y^{2-} or HY^{3-}) at pH 3–10, to the channels in the Nf film. At [EDTA] < 2 mM, not enough EDTA molecules may be present around the sensitizer molecules anchored within the Nf film because of the electrostatic repulsion between EDTA anions and Nf-sulfonate groups whereas the electrostatic attraction between the EDTA anions and $Ru(bpy)_3^{2+}$ is predominant in the homogeneous solution. The overall sensitization process seems to be efficient only when enough electron donors are available at [EDTA] > 2 mM within the Nf film.

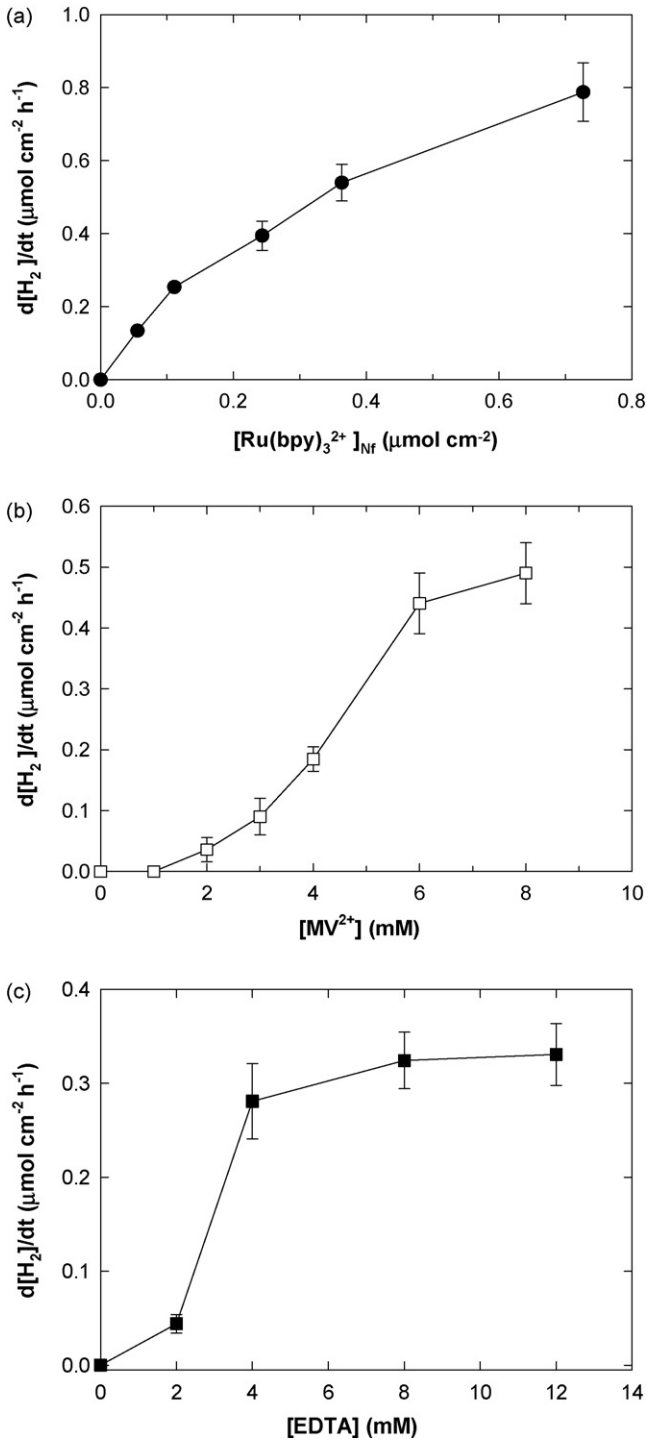

Fig. 5. The hydrogen production rate (averaged over 3–5 h) under visible light as a function of (a) $[Ru(bpy)_3^{2+}]_{Nf}$ (with $[MV^{2+}] = 4$ mM and [EDTA] = 4 mM); (b) $[MV^{2+}]$ (with $[Ru(bpy)_3^{2+}]_{Nf} = 0.24$ μmol/cm^2 and [EDTA] = 4 mM); (c) [EDTA] (with $[Ru(bpy)_3^{2+}]_{Nf} = 0.24$ μmol/cm^2 and $[MV^{2+}] = 4$ mM). $[Pt^0]$ is 14.8 μg/cm^2 for all cases.

3.3. Nafion membrane as a platform of hydrogen generation

The Nafion film has unique properties such as high cation-exchange capacity, nanoporous channel structure for diffusion, high proton activity inside the pores, and chemical and photochemical stability. Such properties of the Nafion film are highly suitable to its utilization as a support for integrating photoactive components for solar hydrogen production.

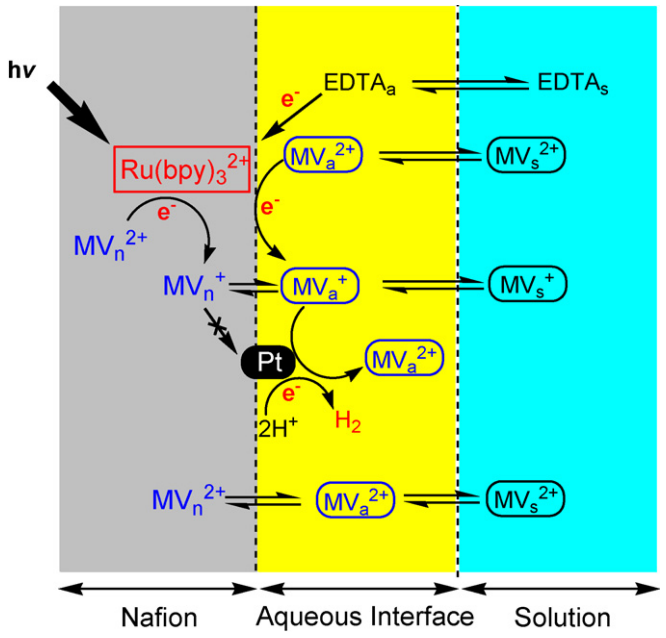

Scheme 3. Schematic diagram of the sensitized production of hydrogen in the Nf film on which photoactive components are immobilized. $Ru(bpy)_3^{2+}$ sensitizers are initially absorbed through ion exchange in the Nf film and Pt particle are deposited on the Nf film surface, whereas MV^{2+} molecules are distributed among the Nf film bulk (MV_n^{2+}), the interfacial region (MV_a^{2+}), and the solution bulk (MV_s^{2+}).

The strongly acidic environment of the Nafion pores, a homologue of perfluorosulfonic superacids [28], provides an ideal condition for hydrogen production. The high proton activity enhances the thermochemical driving force for the electron transfer between MV^+ and H^+. While the reduction potential of protons ($E^\circ(H^+/H_2) = 0.0\,V_{NHE}$) shifts to the positive direction with decreasing pH (Nernstian behavior: −59 mV/pH), the reduction potential of the electron shuttle ($E^\circ(MV^{2+}/MV^+) = -0.44\,V_{NHE}$) is pH-independent. Therefore, the proton reduction by MV^+ should be thermodynamically more favored within the Nf matrix than in the solution bulk.

In {Nf} film, Pt and $Ru(bpy)_3^{2+}$ are immobilized at different sites. Pt particles are mostly on the external surface of the film as Fig. 1 and Scheme 2 show while $Ru(bpy)_3^{2+}$ sensitizers are primarily bound around the sulfonate site in the inner channel along with a minor fraction located at the external Nafion film. Thus there are two electron-transfer pathways from the bound $Ru(bpy)_3^{2+*}$ to the surface Pt site: via $Ru(bpy)_3^{3+}/Ru(bpy)_3^{2+}$ shuttle vs. via MV^{2+}/MV^+ shuttle. Although the electron transfer between $Ru(bpy)_3^{2+}$ and $Ru(bpy)_3^{3+}$ (i.e., self-quenching or self-exchanging) is likely to happen by electron hopping and molecular diffusion [29], the apparent electron transfer rate between the bound redox molecules in polymer films was estimated to be lower by 4–5 orders of magnitude than that in aqueous solution [30]. Therefore, the efficient electron transfer from $Ru(bpy)_3^{2+*}$ to Pt via the $Ru(bpy)_3^{3+}/Ru(bpy)_3^{2+}$ shuttle is limited and needs the presence of the unbound electron-relay like MV^{2+} (see Scheme 3). The lifetime of the triplet excited state of $Ru(bpy)_3^{2+*}$ in wet Nf membrane was measured to be around 900–1200 ns, which is longer than that in water (598 ns) or dried Nafion (600 ns). Thus, the chance of the electron transfer from $Ru(bpy)_3^{2+*}$ to nearby MV^{2+} molecules is higher in Nf film. With $[MV^{2+}] < 1$ mM, almost all MV^{2+} ions are bound at the ion-exchange site and do not properly function as an electron shuttle (Scheme 3). To further test whether the bound MV^{2+} can be effective as an electron shuttle, we prepared MV^{2+}-preadsorbed $\{Ru^{II}/MV^{2+}/Pt/Nf\}$ film and immersed it in EDTA solution (without MV^{2+}). There was no hydrogen production observed under visible-light irradiation,

which verifies that acting electron shuttles should be unbound. The self-exchange rate between MV^{2+} and MV^{+} decreases by ca. four orders of magnitude in the Nafion film as compared to that in the aqueous solution [31]. This indicates the electron transfer is achieved mainly by the molecular diffusion of the MV^{2+}/MV^{+} in the Nafion. Enough free electron shuttles are available only above $[MV^{2+}] > 4$ mM (see Fig. 5b). The electron-mediating action of MV^{2+} seems to be also related with the induction period for hydrogen production observed in $\{Ru^{II}/Pt/Nf\}$ system (see Fig. 4a). In this heterogenized system, the hydrogen evolution was always preceded by the blue coloration of the solution containing $\{Ru^{II}/Pt/Nf\}$ film, which indicates both that MV^{+} diffuses out of the Nf film and that the diffused-out MV^{+} initiates the production of hydrogen at the Pt site on the external surface of Nafion film. Since MV^{+} should be generated in the film bulk where most sensitizers are anchored, the hydrogen production does not start until enough MV^{+} ions accumulate and diffuse out to the external surface where the active Pt is available.

4. Conclusion

The photoactive components-loaded Nafion film successfully produced molecular hydrogen under visible-light irradiation. Although this study deals with a well-known combination of sensitizer, electron relay, and electron donor for hydrogen production, integrating these components within a polymer membrane presents a different and uninvestigated problem. Nafion provides a unique local environment in which all the key processes such as components immobilization, light absorption, charge separation/transfer, and hydrogen production coincide. The present example employing Nafion, $Ru(bpy)_3{}^{2+}$, MV^{2+}, and Pt as main components can be considered as a basic model for the development of H_2-generating film solar reactor and can be further modified by changing the kind of sensitizers, ion-exchange resins, electron shuttles, and cocatalysts for better efficiency and lower cost. The film-type solar hydrogen reactor is ideally suited to harvesting solar energy over the large surface area.

Acknowledgements

This work was supported by KOSEF grant funded by the Korea government (MEST) (No. R0A-2008-000-20068-0), the KOSEF EPB center (Grant No. R11-2008-052-02002), and the Brain Korea 21 program.

Appendix A. Supplementary data

Supplementary data associated with this article can be found, in the online version, at doi:10.1016/j.jphotochem.2008.12.025.

References

[1] K. Kalyanasundaram, Coord. Chem. Rev. 46 (1982) 159–244.
[2] A. Juris, V. Balzani, F. Barigelletti, S. Campagna, P. Belser, A. Vonzelewsky, Coord. Chem. Rev. 84 (1988) 85–277.
[3] T. Abe, M. Kaneko, Prog. Polym. Sci. 28 (2003) 1441–1488.
[4] M.R. Hoffmann, S.T. Martin, W. Choi, D.W. Bahnemann, Chem. Rev. 95 (1995) 69–96.
[5] Z.G. Zou, J.H. Ye, K. Sayama, H. Arakawa, Nature 414 (2001) 625–627.
[6] J. Kiwi, M. Gratzel, J. Am. Chem. Soc. 101 (1979) 7214–7217.
[7] D. Miller, G. McLendon, Inorg. Chem. 20 (1981) 950–953.
[8] E. Bae, W. Choi, J.W. Park, H.S. Shin, S.B. Kim, J.S. Lee, J. Phys. Chem. B 108 (2004) 14093–14101.
[9] D.N. Furlong, D. Wells, W.H.F. Sasse, J. Phys. Chem. 90 (1986) 1107–1115.
[10] D.M. Roundhill, Photochemistry and Photophysics of Metal Complexes, Plenum Press, New York, 1994.
[11] M. Chanon, Homogeneous Photocatalysis, Wiley, 1997.
[12] M. Kaneko, J. Motoyoshi, A. Yamada, Nature 285 (1980) 468–470.
[13] C.K. Gratzel, M. Gratzel, J. Phys. Chem. 86 (1982) 2710–2714.
[14] Y. Kurimura, M. Nagashima, K. Takato, E. Tsuchida, M. Kaneko, A. Yamada, J. Phys. Chem. 86 (1982) 2432–2437.
[15] J. Rabani, M. Kaneko, A. Kira, Langmuir 7 (1991) 941–946.
[16] A. Safranj, S. Gershuni, J. Rabani, Langmuir 9 (1993) 3676–3681.
[17] R.J. Lin, T. Onikubo, K. Nagai, M. Kaneko, J. Electroanal. Chem. 348 (1993) 189–199.
[18] H. Shiroishi, T. Shoji, M. Kaneko, J. Mol. Catal. A: Chem. 187 (2002) 47–54.
[19] T. Hirose, Y. Maeno, Y. Himeda, J. Mol. Catal. A: Chem. 193 (2003) 27–32.
[20] P.C. Lee, D. Meisel, J. Am. Chem. Soc. 102 (1980) 5477–5481.
[21] P.X. He, X.M. Chen, J. Electroanal. Chem. 256 (1988) 353–360.
[22] H.N. Choi, S.H. Cho, W.Y. Lee, Anal. Chem. 75 (2003) 4250–4256.
[23] C. HeitnerWirguin, J. Membr. Sci. 120 (1996) 1–33.
[24] H. Park, W. Choi, J. Phys. Chem. B 109 (2005) 11667–11674.
[25] H. Park, W. Choi, Langmuir 22 (2006) 2906–2911.
[26] M. Kaneko, A. Yamada, in: J.E. Sheats, C.E. Carraher Jr., C.U. Pittman Jr. (Eds.), Metal-Containing Polymeric Systems, Plenum Press, New York, 1985.
[27] H.G. Heller, J.R. Langan, J. Chem. Soc., Perkin Trans. 2 (1981) 341.
[28] G.A. Olah, G.K. Surya Prakash, J. Sommer, Science 206 (1979) 13–20.
[29] H.S. White, J. Leddy, A.J. Bard, J. Am. Chem. Soc. 104 (1982) 4811–4817.
[30] C.R. Martin, I. Rubinstein, A.J. Bard, J. Am. Chem. Soc. 104 (1982) 4817–4824.
[31] J.G. Gaudiello, P.K. Ghosh, A.J. Bard, J. Am. Chem. Soc. 107 (1985) 3027–3032.